

Evaluating The Explainability of State-of-the-Art Deep Learning-based Network Intrusion Detection Systems

Ayush Kumar and Vrizlynn L.L. Thing
 Cyber Security Strategic Technology Centre
 Singapore Technologies Engineering
 Email: ayush.kumar@u.nus.edu, vriz@ieee.org

Abstract—Network Intrusion Detection Systems (NIDSs) which use deep learning (DL) models achieve high detection performance and accuracy while avoiding dependence on fixed signatures extracted from attack artifacts. However, there is a noticeable hesitance among network security experts and practitioners when it comes to deploying DL-based NIDSs in real-world production environments due to their black-box nature, i.e., how and why the underlying models make their decisions. In this work, we analyze state-of-the-art DL-based NIDS models using explainable AI (xAI) techniques (e.g., TRUSTEE, SHAP) through extensive experiments with two different attack datasets. Using the explanations generated for the models’ decisions, the most prominent features used by each NIDS model considered are presented. We compare the explanations generated across xAI methods for a given NIDS model as well as the explanations generated across the NIDS models for a given xAI method. Finally, we evaluate the vulnerability of each NIDS model to inductive bias (artifacts learnt from training data). The results show that: (1) some DL-based NIDS models can be better explained than other models, (2) xAI explanations are in conflict for most of the NIDS models considered in this work and (3) some NIDS models are more vulnerable to inductive bias than other models.

Index Terms—Network Intrusion Detection Systems, NIDS, Machine Learning, explainable Artificial Intelligence, xAI

I. INTRODUCTION

Securing networks against intrusion is paramount, and network intrusion detection systems (NIDS) play a pivotal role in achieving this. Traditionally, NIDSs have relied heavily on signature-based methods [1], [2]- essentially matching attack patterns to known signatures. However, these approaches demand significant manual effort from experts to create and maintain those signatures. Moreover, they fall short when it comes to identifying novel, previously unseen attacks. With the introduction of deep learning (DL)-based NIDSs which leverage DL models to enhance existing defenses, impressive performance and accuracy has been achieved [3], [4] and they have been found to perform better than conventional machine learning (ML) algorithms [5]. In fact, unsupervised DL-based NIDSs can even raise alerts for hitherto unknown attacks. Thanks to these advantages and the rapid evolution of DL techniques, DL-based NIDSs have made significant strides in recent years.

Despite the promise of DL-based NIDSs, there is a noticeable hesitance among network security experts and practitioners when it comes to deploying them in real-world production environments [6]. The crux of the issue lies in the black-box nature of many of these proposed solutions. Essentially, their inner workings (how and why they make decisions) remain elusive, unlike simpler but less effective rule-based approaches that security professionals are accustomed to. Security analysts rely on DL-based NIDSs for critical decisions. However, without clear explanations for the decisions made by these underlying DL models, it becomes difficult for the analysts to trust them. Moreover, DL often operates as a black box within the NIDS. Consequently, hidden correlations stemming from unrelated artifacts can slip past undetected, leading to a flawed perception of the system’s capabilities. Explanation tools and techniques can unveil those hidden correlations, allowing practitioners to assess their impact on the NIDS’s overall effectiveness. As it stands, the current state-of-the-art DL-based NIDSs lack inherent explainability. Therefore, there is a pressing need to scrutinize them using these very explanation techniques.

In this work, we analyze state-of-the-art DL-based NIDS models using explainable AI (xAI) techniques (e.g., TRUSTEE [7], SHAP [8]). Except Kitsune, other NIDS source codes do not provide trained ML models or training/test data in a format which can be directly input to the xAI methods’ APIs. Therefore, we make changes in the NIDS source codes to satisfy the APIs’ requirements. Through extensive experiments with two different attack datasets and using both global explanations and local explanations for the models’ decisions, the most prominent features used by each DL-based NIDS model considered are presented. We compare the explanations generated across xAI methods for a given NIDS model (using our proposed metric) as well as the explanations generated across the NIDS models for a given xAI method (using standard evaluation metrics). Finally, we evaluate the vulnerability of each NIDS model to inductive bias (artifacts learnt from training data). To the best of our knowledge, our work is the first one to generate explanations for state-of-the-art DL-based NIDSs other than Kitsune using xAI techniques.

The main contributions of our work are as follows:

- We analyze state-of-the-art DL-based NIDS models using explainable AI techniques.

- We present the most prominent features used by each NIDS model to make decisions on input data samples using the explanations generated earlier.
- Using the same explanations and some evaluation metrics, we illustrate that:
 - Some DL-based NIDS models can be better explained (in terms of interpretable decision trees) than other models.
 - xAI explanations generated using different tools (e.g., TRUSTEE, SHAP) are in conflict with each other for most of the NIDS models considered.
 - Some NIDS models are more vulnerable to inductive bias (in terms of learnt packet rates) than other models.

The rest of the paper is organized as follows. In Section II, we review published research on the need for explanation of ML systems targeted at cybersecurity, evaluation of explanation methods on DL-based security systems and explainable DL-based attack detection. In Section III, we present a background on the types of explanation methods for ML models, prominent black-box xAI methods, and an overview of the state-of-the-art DL-based NIDSs to which we apply explanation techniques in this work. In Section IV, we explain the issues with applying xAI methods to the DL-based NIDSs directly using their open-source implementations, our approach to addressing those issues and details of our investigation beyond direct application of xAI methods which covers the relation between explanations generated by different xAI methods and the detection of inductive bias in the DL-based NIDSs under consideration in this work. Finally, in Section V, we evaluate the explanations generated for each of the NIDSs using xAI methods, compare the explanations across the NIDS models as well across xAI methods, and discuss insights gleaned from the main results obtained thus far.

II. RELATED WORK

Several works have recommended employing explanation techniques for ML systems deployed for cybersecurity. In [6], the authors have recommended employing explanation techniques to delve deeper into the features of learning-based security systems. Notwithstanding their limitations, these techniques can unveil spurious correlations and empower experts to evaluate their effect on the security system's features. The authors in [9] have also emphasized the importance of explaining the outcomes produced by ML-based detectors used in security contexts. Beyond mere predictions, a cybersecurity threat detection model can offer valuable insights. By understanding the model's explanations, security practitioners can enhance protection around monitored assets in subsequent executions. Explainability varies in relevance across different domains, but the authors contend that it is crucial for several cybersecurity tasks, enabling the effective application of countermeasures against security threats. The participants (security practitioners) of a survey conducted by the authors of [10] have expressed the view that security solution providers ought to prioritize methods that offer clear explanations to their clients.

As a result, we can see the beginning of efforts in the research community to apply xAI techniques to ML-based secu-

rity systems. A few works [11]–[14] have employed xAI methods such as LIME [15] and SHAP [8] to assess the quality of local/global explanations generated for conventional machine learning classifiers (AdaBoost, k-nearest neighbour, Multi-layer Perceptron, Random Forest, XGBoost, Light Gradient-Boosting Machine, Gradient Boosting Classifier) applied to network intrusion datasets (NSL-KDD dataset [16], CICIDS-2017 [17]) in terms of criteria such as faithfulness, stability, complexity, and sensitivity. In [18], the authors have delved into six explanation methods, evaluating their effectiveness across four security systems described in existing literature. These systems leverage DL techniques to detect Android malware, malicious PDF files and security vulnerabilities. The assessment criteria encompass both general properties of deep learning and domain-specific aspects relevant to security.

The authors in [19] have introduced a framework rooted in SHAP to provide explanations for IDSs. This framework blends both local and global explanations, enhancing the overall interpretability of IDSs. Local explanations shed light on why the ML model employed by a specific IDS reaches particular decisions for individual inputs. Meanwhile, global explanations highlight crucial features extracted from the ML model and elucidate the relationships between feature values and specific attack types. [20] has presented a deep learning-based IDS for IIoT networks consisting of an ensemble of three CNN models and an extreme-learning machine model. The authors have used SHAP and LIME techniques to explain the ensemble detector's decision-making process.

A few works have also proposed ML/DL-based attack detection systems with built-in explainability. In [21], the authors have implemented an xAI solution to provide accurate detection and classification of the DNS-over-HTTPS attacks. It is based on a balanced stacked random forest classifier. The authors have highlighted the underlying feature contributions to provide transparent and explainable results from the model. In [22], the authors have proposed an NIDS for IT networks combining ensemble learning and stacking with a meta-learner (CNN) that works on graphical representation of traffic flows and provides the required explainability level for the decisions made. They also provide visual representations of network anomalies that allows security analysts to interpret and gain insights into the detected network anomalies.

Though not targeted at generating explanations, recent works on adversarial learning in NIDSs aim to generate specific examples/feature vectors which can evade detection. Based on a complete/partial knowledge of the ML model underlying a given NIDS and the features used to train the model, researchers have used existing techniques such as genetic algorithm/particle swarm optimization/generative adversarial networks to generate adversarial examples [23]. An update to that work focuses on restricting the adversarial feature space so that the generated features correspond to functional network packets [24]. It does that by presenting a constrained optimization formulation for perturbing raw packet payloads while avoiding modification to the original packet function. A meta-heuristic inspired by genetic algorithm is proposed to solve the optimization problem. However, these works do not offer an explanation as to why the adversarial

examples generated cause mis-classification by the underlying ML model.

Despite the presence of existing works on assessing the explainability of ML/DL and ensemble learning-based NIDSs, our work fills an important gap due to the following reasons:

- Existing works that evaluate xAI methods on ML/DL-based NIDSs ([11]–[14], [20], [22]): (1) do not compare the explainability of those NIDSs with that of state-of-the-art NIDSs and (2) do not include the latest xAI tools for ML/DL-based network security such as TRUSTEE [7].
- Existing explainable-by-design AI-based attack/intrusion detection systems such as [21] are targeted at specific attacks (DNS-over-HTTPS attacks).

III. BACKGROUND

In this paper, since we delve into explaining the decisions of state-of-the-art DL-based NIDSs, it is essential to briefly explore the types of explanation methods present in academic literature, the NIDSs that we consider for explanation in this work and the various aspects of our investigation with xAI techniques on those NIDSs.

A. Explanation Methods- Types

All explanation methods for ML/DL models can be broadly categorized into *black-box* and *white-box* explanations.

Black-box Explanations These methods function within a black-box context, assuming zero knowledge about the inner workings of the underlying ML model and its associated parameters. These methods prove invaluable when direct access to the ML model is not available, for instance, during remote audits of a learning-based application. These black-box methods approximate the underlying ML model’s prediction function f_N , allowing them to estimate how various dimensions of the input vector x affect a given prediction. While they hold promise for explaining deep learning models, their effectiveness can be impeded by the black-box environment, sometimes leaving out crucial insights embedded in the ML model’s parameters and architecture.

White-box Explanations These methods work under the premise that we have full knowledge of all the parameters of the ML model being tested. Armed with this information, these methods bypass approximations and can directly compute explanations for the prediction function, f_N . The same ML model is often used to generate both predictions and explanations, assuming that the model is available on hand. This assumption holds true for stand-alone automated systems such as those that analyse binaries, detect malware or discover software vulnerabilities. However, it is worth noting that some white-box methods are customized for specific neural network architectures deployed in the fields of computer vision/speech processing/natural language processing and may not perform well for other architectures.

B. Prominent Black-box XAI Tools

DL-based NIDS products are expected to be used by end users/customers who do not have access to the ML model

and its parameters underlying the NIDS. This is to maintain confidentiality of the NIDS implementation by the cybersecurity services vendor. Therefore, we assume that the DL-based NIDSs being explained in this work are available to us as a black-box system only and we use xAI techniques designed to explain such black-box ML systems. In what follows, we present a brief overview of each black-box xAI tool that we have tested with as part of this work.

Overview of TRUSTEE: TRUSTEE [7] is a state-of-the-art interpretability tool for ML/DL-based security solutions which generates interpretable decision trees (DT) for a given ML/DL model. It can be used to find out inductive biases in black-box models (e.g., shortcut learning, spurious correlations, sensitiveness to out-of-distribution samples). While generating DT, TRUSTEE focuses on the following desirable properties: model-agnosticism (should be applicable to any given black-box model), model fidelity (how accurate the DT is with respect to the original ML model), model stability (the decision rules should correctly describe how the given black-box model makes a significant number of its decisions and should be largely insensitive to the particular data samples that TRUSTEE used in the process of selecting its final DT explanation) and model complexity (decision rules should be readily recognizable by domain experts). The important aspects of generated DT explanation are summarized in a trust report which helps end users determine whether the given black-box model suffers from the problem of underspecification and can be trusted.

Overview of LIME: Ribeiro et al. [15] introduced LIME, one of the first black-box methods for explaining neural networks that is further extended by SHAP [8]. Both works are motivated by the need to allow users to be able to trust ML models as well as their predictions. LIME is designed to explain the predictions of any classifier or regressor in a faithful way, by approximating it locally with an interpretable model. The main characteristics of LIME are:

- Interpretable, i.e., it provides qualitative understanding of the relation between the input variables and the response.
- Locally faithful, i.e., it corresponds to how the model behaves in the vicinity of the instance being predicted.
- Model-agnostic, i.e., it treats the original ML model as a black box.

LIME aims at approximating the decision function, f of the model being explained by solving the following optimization problem:

$$\underset{g \in \mathcal{G}}{\operatorname{argmin}} \mathcal{L}(f, g, \pi_x), \quad (1)$$

where $\mathcal{L}(f, g, \pi_x)$ is the fidelity function which is a measure of how unfaithful the interpretable model g is in approximating f in the locality defined by π_x , while $\pi_x(z)$ is the proximity measure between an instance z to x , so as to define the locality around x and x is the input to f .

Overview of SHAP: SHAP [8] (SHapley Additive exPlanations) subsumes additive feature attribution methods such as LIME and uses the following forms for $\mathcal{L}(f, g, \pi_x)$ and π_x

under the SHAP kernel method, which is shown to recover Shapley Values [25] when solving the regression:

$$\begin{aligned} \mathcal{L}(f, g, \pi_{x'}) &= \sum_{z' \in Z} [h_x^{-1}(z') - g(z')]^2 \pi_{x'}(z'), \\ \pi_{x'}(z') &= \frac{M - 1}{\binom{M}{|z'|} |z'| (M - |z'|)} \end{aligned}$$

where x' is the simplified input which maps to the original input x through a mapping function $x = h_x(x')$, M is the number of simplified input features, $z' \in \{0, 1\}^M$, and $|z'|$ is the number of non-zero elements in z' .

Shapley values are a concept from game theory where the features act as players under the objective of finding a fair contribution of the features to the payout, in this case the prediction of the model. Different from TRUSTEE, Shapley values are used for local interpretation. In other words, it is used to interpret how a prediction result is reached for a specific data sample or subset of samples. Specifically, Shapley values can tell how each feature contributes to the predicted results. A positive Shapley value means that the feature's value pushes the classification result toward being malicious, and a negative Shapley value does the contrary.

Overview of LEMNA: LEMNA [26] is a black-box method specifically designed for security applications. Given an input data instance x and a classifier such as an RNN, this method aims to identify a small set of features that have key contributions to the classification of x . This is done by generating a local approximation of the target classifier's decision boundary near x . It uses a mixture regression model (to approximate locally non-linear decision boundaries) enhanced by fused lasso (to handle correlated features) for approximation. The mixture regression model is a weighted sum of K linear regression models:

$$f(x) = \sum_{j=1}^K \pi_j (\beta_j \cdot x + \varepsilon_j). \quad (2)$$

The parameter K specifies the number of models, the random variables $\varepsilon = (\varepsilon_1, \dots, \varepsilon_K)$ originate from a normal distribution $\varepsilon_i \sim \mathcal{N}(0, \sigma)$ and $\pi = (\pi_1, \dots, \pi_K)$ holds the weights for each model. The variables β_1, \dots, β_K are the regression coefficients and can be interpreted as K linear approximations of the decision boundary near $f(x)$.

xAI Evaluation Metrics: Several metrics have been proposed in literature to quantify the effectiveness of xAI techniques. The authors in [27] have categorized existing xAI evaluation metrics into *subjective* and *objective* metrics. Subjective metrics rely on human feedback, e.g., comprehensibility, satisfaction, and persuasiveness. This feedback can come from randomly selected users or domain experts. Objective metrics are grounded in formal definitions, e.g., explanation completeness which quantifies the extent to which a prediction's contributing features are captured, and perturbation metrics which assess sensitivity to input changes by comparing outputs and considering model parameter variations across different instances of the same model.

C. State-of-the-art Deep Learning-based NIDSs

We now present a brief overview of state-of-the-art DL-based NIDSs that we have considered in this work.

Kitsune [5] proposes an online unsupervised anomaly detection system based on an ensemble of autoencoders which is lightweight in terms of memory footprint and meant to be deployed on network gateways and routers to detect attacks on the local network. It uses a damped incremental statistics (DIS) method to extract network traffic features which has the advantage of extracting features from dynamic network traffic at high speed.

HorusEye [28] is a two-stage anomaly detection framework for IoT. In the first stage (Gulliver Tunnel), preliminary burst-level anomaly detection is implemented on the data plane using an isolation forest model converted into a set of white-listing rules. The suspicious traffic is then reported to the control plane for further investigation. To reduce the false positive rate, the control plane carries out the second stage (Magnifier), where more thorough anomaly detection is performed over the reported suspicious traffic using Kitsune DIS features and an asymmetric autoencoder with separable and dilated convolutions.

ENIDrift [29] addresses real-world issues in DL-based NIDS deployment such as concept drift (change in statistical properties of target variable over time), class-imbalanced training data and well-crafted ML attacks (training data contamination, adversarial attacks). It includes three main components: iP2V- an incremental feature extraction method based on Word2Vec, an ensemble of autoencoders, a sub-classifier generation module and an update module.

HELAD [30] uses ensemble learning consisting of an unsupervised autoencoder as a base learner which learns the profile for normal network traffic and a supervised LSTM (Long-term short-term memory) which is trained using the autoencoder's output to detect continuous attacks. The model is re-trained using a new concept of time slice re-training. It also uses dynamic thresholds and integrated learning parameters to keep the anomaly detection performance from degradation.

The above state-of-the-art systems were selected since: (1) they were published in prominent avenues (NDSS, USENIX Security, ACSAC) and include works published as recently as 2023, (2) provide a clear performance comparison with Kitsune (which is the most cited deep learning-based NIDS with an open-source implementation) and (3) they cover a diverse ground on the application of deep learning in network intrusion detection. Kitsune uses an ensemble of autoencoders while ENIDrift builds on top of that by including a sub-classifier generation and update module to address concept drift in real-world networks. HorusEye's Magnifier switches the ensemble of autoencoders for a single asymmetric autoencoder to keep the solution lightweight and reduce the false-positive rate. HELAD uses a single autoencoder as well but combines it with an LSTM network.

IV. xAI ANALYSIS OF DEEP LEARNING-BASED NIDSs

In this work, we analyze four state-of-the-art DL-based NIDSs (Kitsune, HorusEye, ENIDrift, HELAD) using xAI

techniques. However, xAI techniques such as TRUSTEE and kernel SHAP can not be applied directly to the NIDSs under consideration. This is because xAI methods have certain requirements at the API level which are not fulfilled by the current implementations of the NIDSs. We had to modify the NIDS implementations to make them compatible with xAI methods. Still, there were a few xAI methods whose requirements were found to be incompatible with the NIDS implementations unless we made major changes to the source code. Additionally, we did not limit ourselves to a direct application of xAI methods to the NIDSs but we also investigated: (1) the relation between the explanations generated for a given NIDS by different xAI methods, and (2) the presence of inductive biases in the NIDS implementations.

A. xAI-compatible NIDS Implementation

The TRUSTEE trust report generating API has two requirements: (1) a trained ML/DL model with a *predict()* function taking training/test dataset as the only input and outputting predicted labels, and (2) training/test datasets and corresponding predicted labels should be in *numpy array/pandas dataframe* format. The kernel SHAP API shares the requirements of TRUSTEE API. Except Kitsune, other NIDS source codes do not provide trained ML model or training/test data in a format which can be directly input to TRUSTEE API or kernel SHAP API.

For example, in the case of ENIDrift source code, the input dataset and predicted labels were not in *numpy array/pandas dataframe* format while the *predict()* function was not designed for an input dataset in the form of a 2-D matrix with rows as samples and columns as feature values. Further, ENIDrift does not extract explicit features from incoming packets but instead embeds packets to vectors which may not be meaningful for model explainability analysis. In the case of HorusEye source code, the main script was in the form of a command with argument parsing, all library functions were defined in the same main script, there was no *predict()* function and input dataset and predicted labels were not in *numpy array/pandas dataframe* format. In the case of HELAD source code, there was no *predict()* function implemented and the NIDS model returned anomaly scores instead of class labels. Further, the way anomaly scores were calculated was not compatible with TRUSTEE API implementation.

While running LIME analysis of above NIDSs, we received an error that LIME does not support ML/DL models which do not have *predict_proba()* function implemented. Since all the state-of-the-art DL-based NIDSs considered in this paper do not implement *predict_proba()* function, we are forced to leave out LIME analysis of the NIDSs from this paper. Here, *predict_proba()* function returns the predicted probabilities of the input features belonging to each category. This method, instead of returning a discrete class, returns the probabilities associated with each class. This is useful when we not only want to know the predicted category of the input features, but also the model's confidence in its prediction.

While running LEMNA analysis of above NIDSs, we found that the current implementation (last changed 5 years ago) only

supports basic MLP, CNN and RNN models. Custom ML/DL models such as the NIDS models which are under consideration in this work are not supported. Further, LEMNA does not output feature-based model explanations for processing by cybersecurity experts such as those offered by TRUSTEE and SHAP.

B. Investigation Beyond Direct xAI Analysis

Relation between TRUSTEE and SHAP Interpretations:

To establish the relationship between TRUSTEE global explanations and the SHAP local explanations of the black-box model underlying a given NIDS, we can follow two approaches:

- *Naïve approach*- We can directly compare the kernel SHAP features with highest SHAP values against the top-k features identified by TRUSTEE report. However, this comparison would not be meaningful as the SHAP value for each feature is calculated for a subset of data samples and reflects the importance of that feature in the decision made by the black-box model for a majority of the data samples in that subset. On the other hand, TRUSTEE acts on the complete input dataset and identifies the top features contributing the most to forming the decision boundary separating all benign and malicious data samples which are part of the input dataset.
- *Systematic approach*- Since xAI methods such as SHAP are more suited towards analyzing a subset of data samples [7], they can be applied to the subset of samples corresponding to a path in a TRUSTEE DT starting at the root node and ending at one of the leaf nodes. We can compare the explanation thus generated with the one provided by TRUSTEE.

Under the systematic approach, for a given subset of data samples D , if T is the set of features used in the selected root node-leaf node DT path decisions and S is the set of features identified by kernel SHAP that contribute most to the classification decision for majority of the samples in D , then $T \subset S$ should hold true for the TRUSTEE DT explanation to agree with the SHAP explanation of the black-box model at the subset level. To form the set of features S , the mean absolute value of kernel SHAP values for multiple data samples are calculated for every feature, and subsequently the features are ranked according to their aggregate SHAP values to find the top features. For a black-box NIDS model, the local explanation (SHAP) may agree with the global explanation (TRUSTEE) depending on the data subset on which they are executed. However, not all local explanations may agree with the global explanation. To evaluate the level of agreement between TRUSTEE and SHAP for an NIDS trained on a given dataset, we propose the following approach:

- 1) Sample different subsets from the original evaluation dataset by selecting different root node-leaf node paths in the TRUSTEE DT.
- 2) Use each sampled data subset for executing kernel SHAP on the trained NIDS.
- 3) We propose the *TRUSTEE-SHAP agreement score* on a data subset D which can be calculated as:

$$\alpha_{TRUSTEE-SHAP}^D = \frac{n(T \subset S)}{n(T)}, \quad (3)$$

where $n(T \subset S)$ refers to the number of TRUSTEE DT features which are a subset of SHAP features and $n(T)$ is the total number of TRUSTEE DT features corresponding to the selected data subset D .

We also define the *m-point average TRUSTEE-SHAP agreement score* for an NIDS as the average of TRUSTEE-SHAP agreement scores for m different data subsets. It can be expressed as:

$$A_{TRUSTEE-SHAP}^m = \frac{1}{m} \sum_m \alpha_{TRUSTEE-SHAP}^{D_m} \quad (4)$$

Inductive Bias: A number of ML/DL models face the issue of underspecification. This term refers to the challenge of determining whether a model’s high performance is due to its genuine ability to capture essential patterns in the data or merely the result of certain inductive biases it has learned. These biases often appear as spurious correlations, a lack of ability to adapt to data samples with variable statistics, shortcut learning strategies, etc. The presence of such biases in trained models undermines their reliability and expected performance in real-world applications. Therefore, identifying these inductive biases is crucial for establishing trust in ML/DL models. To detect the presence of an inductive bias in the DL-based NIDSs under consideration in this work, such as vulnerability to variable packet rate samples, we use tampered malicious traffic traces [7] which alter the attack segments of the original traffic traces by distributing the malicious packets in such a way that the packet rate remains within a specified limit.

V. EXPERIMENTAL RESULTS

In this section, we present explanations of state-of-the-art DL-based NIDSs generated using xAI methods such as TRUSTEE and kernel SHAP. For each pair of NIDS and xAI method, we wrote Python scripts for generating the explanation using the xAI method’s API and the modified source code of the NIDS (to make it compatible with the xAI method’s API implementation). Using the generated explanations, we present the most prominent features used by each NIDS model to make decisions on input data samples. We also investigate the relation between the explanations generated for a given NIDS by TRUSTEE and kernel SHAP by using the systematic approach for comparing TRUSTEE and SHAP explanations at the DT subset-level as explained in sub-section IV-B. Subsequently, we investigate the presence of inductive biases (e.g., vulnerability to variable packet rate samples) in the NIDS implementations using tampered malicious traffic traces as explained in sub-section IV-B. Finally, we compare the explanations generated across the four NIDSs by TRUSTEE using the fidelity metric and by kernel SHAP using general xAI evaluation metrics.

NIDSs Evaluated: We have used all the state-of-the-art DL-based NIDSs presented in Section III-C (Kitsune, HorusEye, ENIDrift and HELAD) for our analysis. When we refer to HorusEye from this point onwards, we are referring to its

Magnifier component which performs deep learning-based anomaly detection.

Datasets: We use the Kitsune Mirai dataset [5] and the CICIDS-2017 dataset [17] for training/testing the DL-based NIDSs under consideration. The Mirai PCAP trace consists of $\sim 760k$ packets of synthetically generated attack in a network with nine IoT devices, first $\sim 120k$ packets consist of benign traffic, remaining $\sim 640k$ packets have anomalous traffic. We use the Kitsune code to extract features from the PCAP trace through the DIS method. The CICIDS-2017 dataset [17] consists of five days of packet capture (July 3 to July 7, 2017) from a small-scale enterprise-like network, with the first day consisting of benign background traffic and the other days consisting of attack traffic (brute force SSH, DoS, Heartbleed, web attack, infiltration, etc.). It consists of significant drift over the data collection period in terms of different attack tools used. The CICIDS-2017 dataset provides PCAP traces, labeled network traffic flows and CSV files consisting of pre-selected features extracted from traffic flows. We use the raw PCAP traces directly and extract features from them using the Kitsune DIS method to maintain consistency. Below, we present the results using Mirai dataset only. Since the results obtained with CICIDS-2017 dataset are similar to those obtained with the Mirai dataset, we include them in the Appendix Section A.

Test Environment: To test Kitsune, HorusEye and ENIDrift NIDSs with xAI methods, we used a VMWare ESXi server VM with Intel Xeon Silver 4216 CPU @2.10GHz, 64-bit architecture, 8 cores, 16GB RAM and running Ubuntu 18.04/Ubuntu 20.04 OS. For testing HELAD NIDS, we used an Nvidia RTX 3090 GPU cluster with each GPU @1.4GHz, $\sim 25GB$ of memory since it requires training deep belief networks and LSTMs. Each GPU had 328 tensor cores and was running Ubuntu 22.04 OS.

A. Case Study- Kitsune \times Mirai

TRUSTEE Analysis: The results of TRUSTEE analysis for Kitsune are shown in Table I. The *sample size* refers to the fraction of the training dataset to use to train the student decision tree model. *Fidelity* is defined as the R-squared value between Kitsune’s predictions and those obtained by the DT explanation. Using TRUSTEE with 30% of the original Mirai dataset samples and no pruning results in the DT explanation which achieves 0.786 fidelity compared to Kitsune. Using TRUSTEE with 30% of the dataset samples and top-k pruning method (setting $k = 3$) results in a DT explanation that is shown in Fig. 1 and achieves 0.697 fidelity compared to Kitsune.

Using TRUSTEE with 30% of the dataset samples and top-k pruning method (setting $k = 10$) results in a DT explanation which achieves 0.721 fidelity compared to Kitsune. The reduction in fidelity with pruning branches of a DT is expected since the obtained smaller trees run the risk of missing important decision branches as they prevent the consideration of any further decision branches once the stopping criterion is reached.

The fidelity score presents a way for security practitioners to gauge the effectiveness of the explanation generated for an

NIDS. A security practitioner prioritising just explainability should select the NIDS with the highest fidelity score. However, a typical practitioner interested in deploying a DL-based NIDS will prioritise not just its explainability but also its attack detection performance. Traditionally, the detection performance of ML/DL-based NIDSs has been measured in terms of metrics such as accuracy, precision, recall and F1 score. An example of the metric a security practitioner can use while selecting a DL-based NIDS is a weighted combination of the NIDS’s average F1 score for different kinds of attacks and TRUSTEE fidelity, expressed as below:

$$S = \alpha * (F1 - score) + (1 - \alpha) * (Fidelity), 0 \leq \alpha \leq 1 \quad (5)$$

By varying the value of the weight, α , the security practitioner can prioritise between detection performance and fidelity.

Based on the TRUSTEE analysis results obtained earlier, the top three prominent features that Kitsune uses to determine an anomaly are:

- *HpHp_0.01_pcc_0_1*, *HpHp_0.1_pcc_0_1*- Correlation coefficient between two packet size streams aggregated by traffic sent between a set of source and destination IP addresses with time windows 0.01 (1 minute) and 0.1 (10 seconds)
- *HpHp_0.1_weight_0*- Weights (packet count) aggregated by traffic sent between a set of source and destination IP addresses and associated with the time window 0.1 (1.5 seconds).

Thus, Kitsune’s DT relies mainly on the volume of packets and sizes of packets exchanged per time frame to determine if an attack is underway.

Information about the top prominent packet-based features used by a DL-based NIDS for anomaly detection makes it easier for a security practitioner interested in deploying the NIDS to trust their internal decision making process. It also enables practitioners to compare NIDSs based on their respective top features. However, practitioners need to select only those NIDSs for comparison whose fidelity is above a certain minimum threshold. If the fidelity falls below that threshold, it means that the DT explanation generated for the corresponding NIDS is not reliable.

Sample size	Top-k pruning used?	DT size, depth, leaves	Fidelity
30%	No	133377, 70, 66689	0.786
30%	Yes (k=3)	19, 9, 10	0.697
30%	Yes (k=10)	37, 13, 19	0.721

TABLE I: TRUSTEE analysis results for Kitsune Mirai model

SHAP Analysis: Fig. 2 illustrates a local explanation for a benign packet data point using a SHAP’s force plot for Kitsune, displaying the contribution of each feature to the prediction. The plot shows the base value, and the features containing a positive influence on the prediction are in red, and the features showing a negative influence on the predictions are in blue. The base value in the plots is the average of all prediction values. Each strip in the plot illustrates how the features influence the predicted value, either drawing it closer

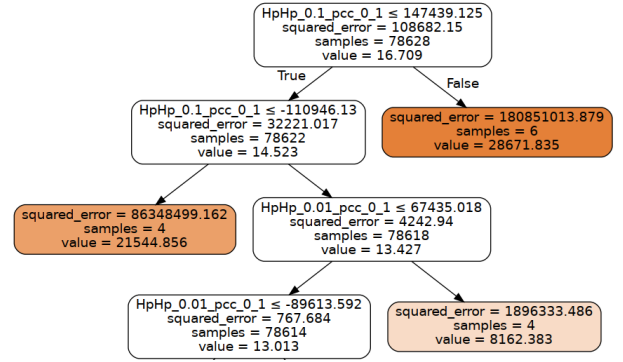


Fig. 1: Decision tree for Kitsune Mirai model with Top-k pruning (k=3). Only the top 3 layers are shown.

or pushing it farther away from the base value. Red strip features push the value to higher values, whereas blue strip features push the value to lower values. The contribution of features holding broader strips is more.

The base value is 0.0646. Features such as *HpHp_0.1_weight_0* and *MI_dir_0.1_weight* have a negative impact on the prediction value. *HpHp_0.1_weight_0* is the most crucial feature, as the contribution has a broader range. The total negative contribution is greater than the positive contribution, and the final predicted value is lesser than the base value. As a result, the class is predicted as benign. The feature *HpHp_0.1_weight_0* corresponds to weights aggregated by traffic sent between a set of source and destination IP addresses using a specific protocol (ARP/TCP/UDP) with time window 0.1 (10 seconds) while the feature *MI_dir_0.1_weight* corresponds to weights aggregated by source MAC and IP addresses, with time window 0.1 (10 seconds).

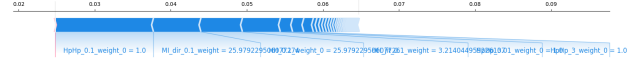


Fig. 2: SHAP force plot for a single data point from Kitsune Mirai model

Using kernel SHAP analysis, Fig. 3 shows a summary of how the top features in Mirai dataset impact the Kitsune NIDS model’s output through a beeswarm plot for randomly selected 1000 data samples corresponding to the benign root node-leaf node path in the TRUSTEE DT (Fig. 1) which takes 625.70 seconds on an average. Running SHAP analysis for the whole dataset will take substantial amount of time and computing resources. Each instance of the given explanation is represented by a single dot on each feature row. The x position of the dot is determined by the SHAP value of that feature, and dots pile up along each feature row to show density. Color is used to display the original value of a feature. The features are ordered using the mean absolute value of the SHAP values for each feature. Features such as *MI_dir_0.1_weight*, *HH_0.01_weight_0* and *HH_0.1_weight_0* have the most impact on the prediction value, in that order. *HH_0.01_weight_0* and *HH_0.1_weight_0* correspond to weights aggregated by traffic sent between a set of source and destination IP addresses with time windows 0.01 (1 minute) and 0.1 (10 seconds) respectively.

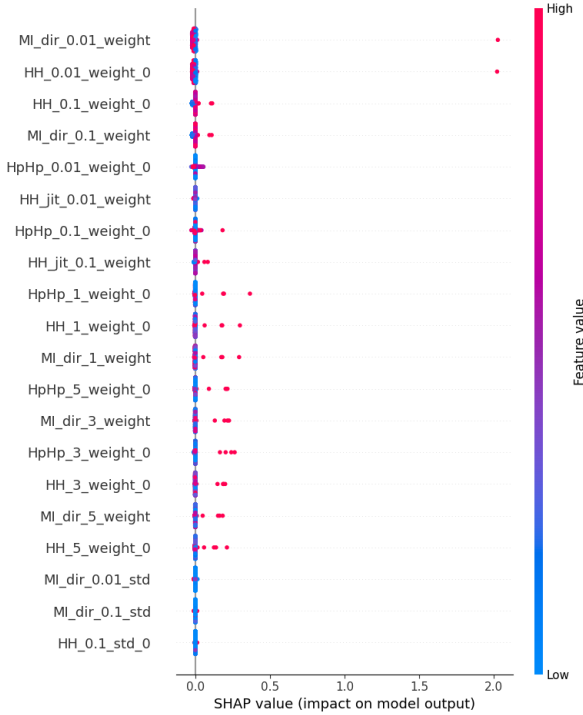


Fig. 3: SHAP beeswarm plot for Kitsune Mirai model

Detection of Inductive Bias: It was shown in [7] that Kitsune NIDS is vulnerable to variable packet rate samples when used with the Mirai dataset introduced in [5]. The authors evaluated the following threshold ranges (in packets per second) for ARP requests originating from devices infected with Mirai: (1) 10-50, (2) 30-70 and (3) 50-90. The original trace as well as the tampered traces are shown in Fig. 4. It can be observed that tampering had a significant effect on the difference between benign and attack traffic in terms of number of packets per second. Kitsune was executed on each trace with an identical number of training samples. The results showed that the RMSE values generated by Kitsune NIDS decreased significantly with a drop in the attack traffic volume, reaching the values corresponding to benign traffic.

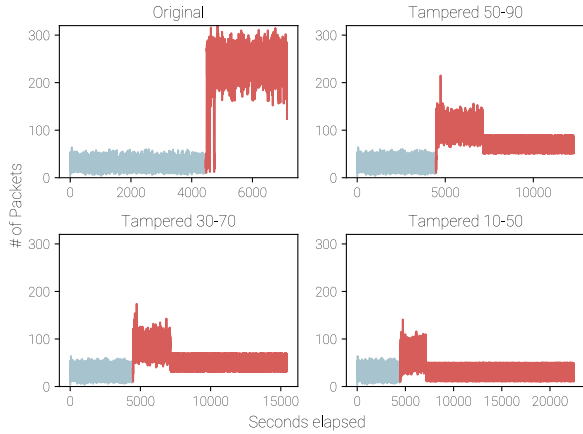


Fig. 4: Number of packets per second for original Kitsune Mirai trace and tampered traces. Blue portions of the plot correspond to benign traffic while red portions correspond to malicious traffic inclusive of benign and attack traffic.

B. Case Study- HorusEye \times Mirai

TRUSTEE Analysis: The results of TRUSTEE analysis for HorusEye are shown in Table II. Using TRUSTEE with 30% of the Mirai dataset samples with no pruning results in a DT explanation which achieves negative fidelity (~ -1.365) compared to original HorusEye model. Using TRUSTEE with 30% of the dataset samples and top-k Pruning method (setting $k = 10$) results in a DT explanation which achieves negative fidelity ($\sim -1.038e - 06$) compared to original HorusEye model. Negative fidelity values mean that the DT explanation fits HorusEye predictions worse than the mean of the predictions.

Nevertheless, the decision tree for HorusEye Mirai model with top-k pruning ($k=10$) is shown in Fig. 5. The top three prominent features that HorusEye’s DT uses to determine an anomaly are:

- 1) $HH_3_pcc_0_1$ - Correlation coefficient between two packet size streams aggregated by traffic sent between a set of source and destination IP addresses with time window 3 (500 milli-seconds).
- 2) $HH_1_std_0$ - Standard deviation of packet sizes aggregated by the traffic sent between a set of source and destination IP addresses with time window 1 (1.5 seconds).
- 3) $MI_dir_0.01_mean$ - Mean of packet sizes aggregated by source MAC and IP addresses, with time window 0.01 (1 minute).

Thus, HorusEye’s DT relies mainly on the sizes of packets exchanged between a pair of IP addresses per time frame to determine if an attack is underway.

Sample size	Top-k pruning used?	DT size, depth, leaves	Fidelity
30%	No	45, 11, 23	-1.365
30%	Yes (k=10)	1, 0, 1	-1.038e-06

TABLE II: TRUSTEE analysis results for HorusEye Mirai model

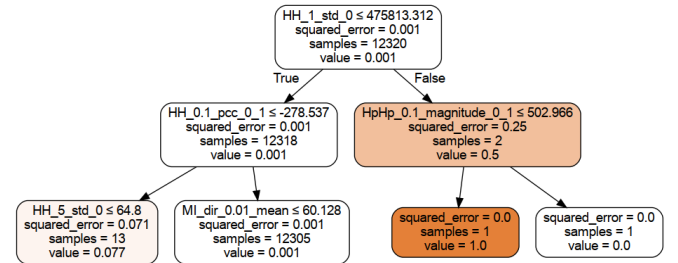


Fig. 5: Decision tree for HorusEye Mirai model with Top-k pruning ($k=10$). Only the top 3 layers are shown.

SHAP Analysis: Using kernel SHAP analysis, Fig. 6 shows a summary of how the top features in Mirai dataset impact the HorusEye NIDS model’s output using a beeswarm plot for randomly selected 1000 data samples corresponding to the benign root node-leaf node path in the TRUSTEE DT (Fig. 5). Features such as $HH_1_std_0$, $HH_5_std_0$ and $HpHp_0.01_magnitude_0_1$ have the most impact on the prediction value, in that order. $HH_1_std_0$ and $HH_5_std_0$ correspond to the standard deviation of packet sizes aggregated

by the traffic sent between a set of source and destination IP addresses with time windows 1 (1.5 seconds) and 5 (100 ms) respectively, while *HpHp_0.01_magnitude_0_1* corresponds to the absolute magnitude of two packet size streams aggregated by the traffic sent between a set of source and destination IP addresses with time window 0.01 (1 minute).

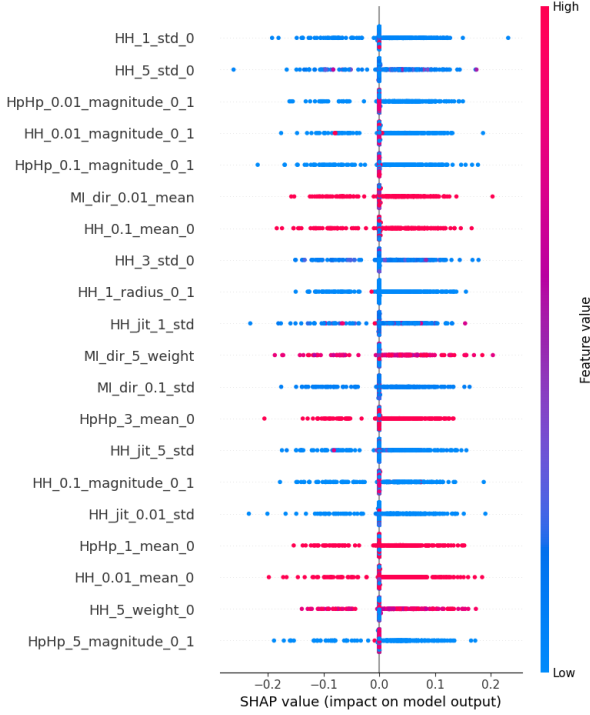
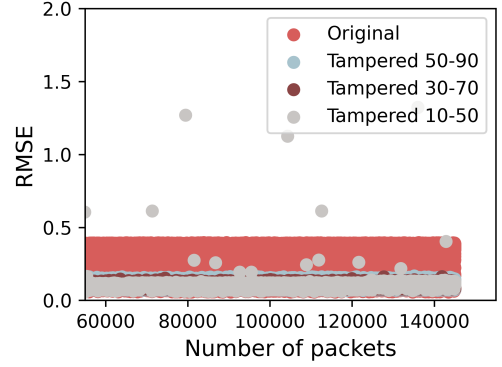


Fig. 6: SHAP beeswarm plot for HorusEye Mirai model

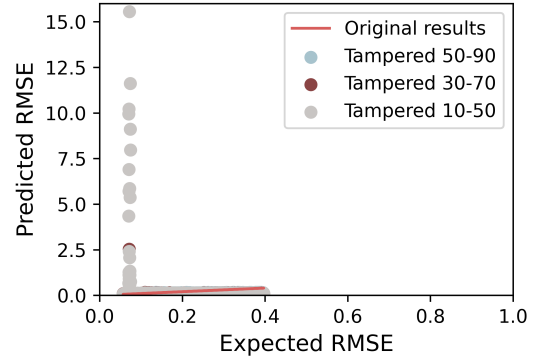
Detection of Inductive Bias: Following a similar approach as the Kitsune case, three separate tampered traces with different attack traffic volumes were obtained from the Mirai dataset and HorusEye was executed on each trace. In Fig. 7a, we show the results for first 200,000 packets of each traces. In Fig. 7b, we also compare the expected RMSE (produced by HorusEye in the original trace) and the predicted RMSE for each tampered trace. The results show that the RMSE values generated by HorusEye decrease with a drop in the attack traffic volume. However, the difference between the RMSE values produced by the original and tampered traces is not as pronounced as in the case of Kitsune NIDS. This experiment demonstrates that the Mirai use case from HorusEye is vulnerable to variable packet rate samples, though to a lesser extent than Kitsune. It should be noted here that HorusEye [28] authors had recognized this issue (without an empirical analysis though) by stating that the frequency of Mirai attacks is too high in the original dataset to reflect real botnet infection. Therefore, the authors had randomly down-sampled the Mirai attack traffic in Kitsune dataset to consist of 40,000 packets during HorusEye’s performance evaluation.

C. Case Study- ENIDrift × Mirai

TRUSTEE Analysis: The results of TRUSTEE analysis for ENIDrift are shown in Table III. Using TRUSTEE with



(a) Predicted RMSE vs packet count



(b) Predicted vs expected RMSE (produced by HorusEye in the original trace)

Fig. 7: HorusEye RMSE values for the first 200k packets from original and tampered traces.

30% of the Mirai dataset samples and no pruning results in the DT explanation which achieves 0.715 fidelity compared to ENIDrift. Using TRUSTEE with 30% of the dataset samples and top-k Pruning method (setting $k = 10$) results in a DT explanation (shown in Fig. 8) which achieves negative fidelity ($\sim -1.536e-09$) compared to ENIDrift. This is expected since pruning the branches of a DT reduces its fidelity. The most prominent features ENIDrift uses to determine anomaly are f_{44} and f_9 . *ENIDrift does not extract explicit features from incoming packets. Instead, it uses ip2V incremental embedding technique based to embed packets to vectors.* The embedding vector length in ENIDrift implementation is 200.

Sample size	Top-k pruning used?	DT size, depth, leaves	Fidelity
30%	No	5, 2, 3	0.715
30%	Yes (k=10)	1, 0, 1	-1.536e-09

TABLE III: TRUSTEE analysis results for ENIDrift Mirai model

SHAP Analysis: Fig. 9 shows a summary of how the top features in Mirai dataset impact the ENIDrift NIDS model’s output using a beeswarm plot for randomly selected 300 data samples. Features (embedding vector components) such as f_{115} , f_{89} , f_{47} have the most impact on the prediction value, in that order.

Detection of Inductive Bias: Following a similar approach as the Kitsune case, three separate tampered traces with differ-

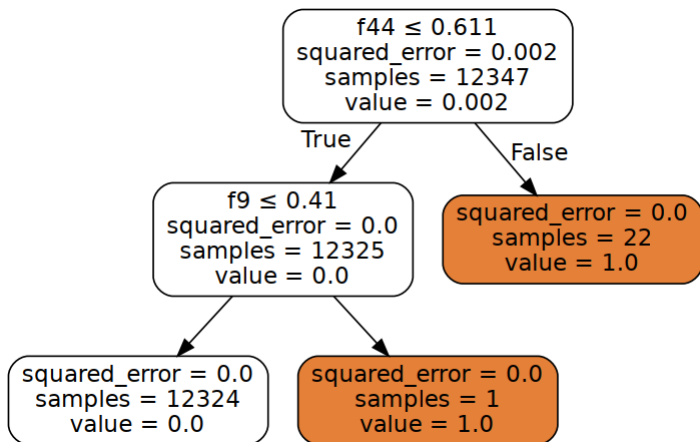


Fig. 8: Decision tree for ENIDrift Mirai model with Top-k pruning ($k=10$).

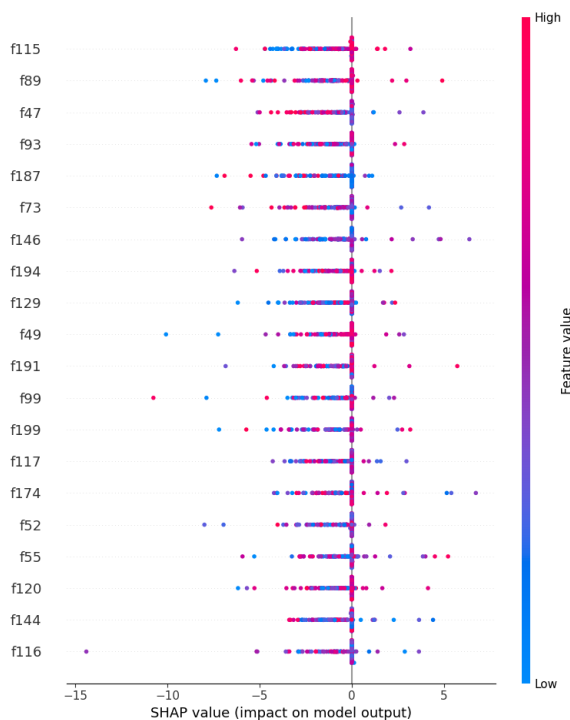
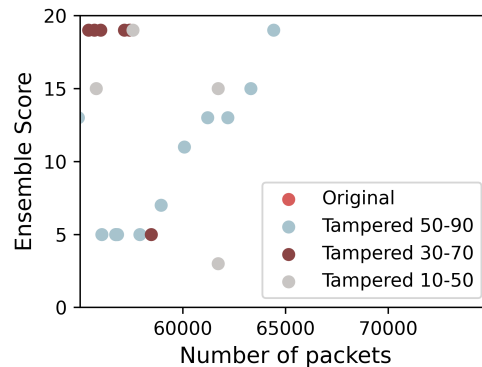
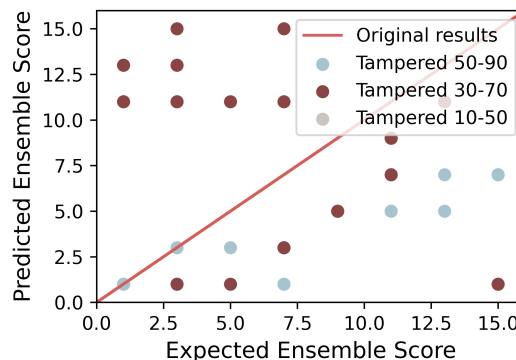


Fig. 9: SHAP beeswarm plot for ENIDrift Mirai model

ent attack traffic volumes were obtained from the Mirai dataset and ENIDrift was executed on each trace. In Fig. 10a, we show the results for first 120,000 packets of each traces. In Fig. 10b, we also compare the expected (weighted) ensemble scores (produced by ENIDrift in the original trace) and the predicted (weighted) ensemble scores for each tampered trace. The results show that the ensemble scores produced by ENIDrift do not have a discernable pattern of dependence on the volume of the attack traffic encountered. Since the distance of the dots for tampered traces from the diagonal line in Fig. 12b does not follow any pattern, the effect that tampering with the Mirai attack traces had on the predicted ensemble scores and hence, whether the Mirai use case from ENIDrift is vulnerable to variable packet rate samples or not, remains inconclusive.



(a) Predicted ensemble score vs packet count



(b) Predicted vs expected ensemble score (produced by ENIDrift in the original trace)

Fig. 10: ENIDrift ensemble scores for the first 120k packets from original and tampered traces.

D. Case Study- HELAD \times Mirai

TRUSTEE Analysis: The results of TRUSTEE analysis for HELAD are shown in Table IV. Using TRUSTEE with 30% of the Mirai dataset samples and no pruning results in the DT explanation which achieves 0.0 fidelity compared to HELAD. Using TRUSTEE with 30% of the dataset samples and top-k Pruning method (setting $k = 10$) results in a DT explanation (shown in Fig. 11) which achieves 0.0 fidelity compared to HELAD. A fidelity value of 0.0 means that the DT explanation fits HELAD predictions only as good as the mean of the predictions.

The top three prominent features HELAD's DT uses to determine an anomaly are:

- 1) *MI_dir_3.0_weight*- Weights aggregated by source MAC and IP addresses, with time window 3.0 (500 milliseconds).
- 2) *HH_1.0_magnitude_0_1*- Absolute magnitude of two packet size streams aggregated by the traffic sent between a set of source and destination IP addresses with time window 1.0 (1.5 seconds).
- 3) *HH_0.01_weight_0*- Weights aggregated by traffic sent between a set of source and destination IP addresses with time window 0.01 (1 minute).

Thus, HELAD's DT relies mainly on the volume of packets and the sizes of packets exchanged between a pair of IP

addresses per time frame to determine if an attack is underway.

Sample size	Top-k pruning used?	DT size, depth, leaves	Fidelity
30%	No	26289, 100, 13145	0.0
30%	Yes (k=10)	435, 94, 218	0.0

TABLE IV: TRUSTEE analysis results for HELAD Mirai model

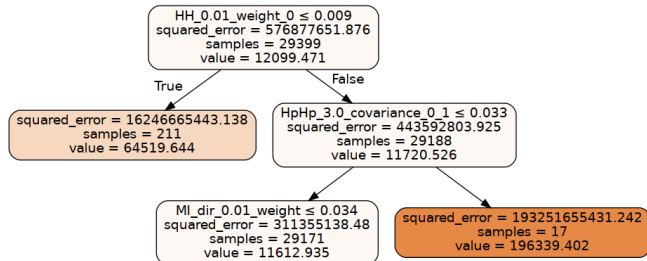


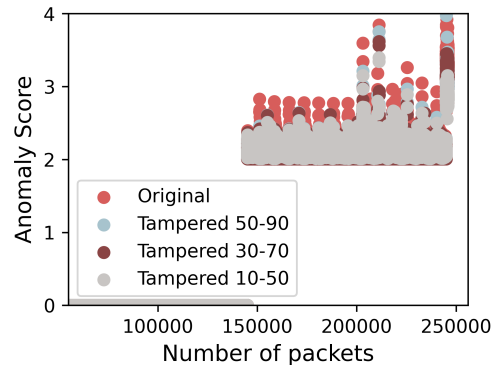
Fig. 11: Decision tree for HELAD Mirai model with Top-k pruning (k=10). Only the top 3 layers are shown.

SHAP Analysis: Running a kernel SHAP analysis of HELAD NIDS with the Mirai dataset resulted in issues. First, we ran the analysis with 200,000 packets but it threw a *numpy* memory error since it was unable to allocate a huge amount of memory (335 GiB) for storing a (2248×20000000) array with 64-bit float values. Next, we ran the analysis with 20,000 packets but the LSTM was taking too long to train. Hence, we decided to not proceed with the kernel SHAP analysis.

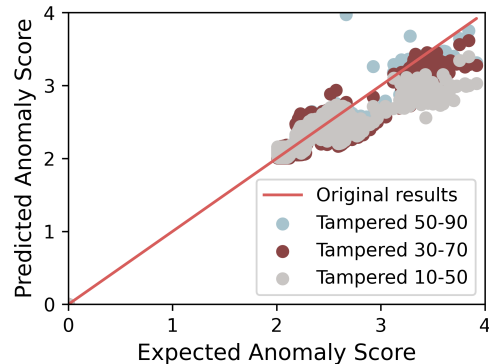
Detection of Inductive Bias: Following a similar approach as the Kitsune case, three separate tampered traces with different attack traffic volumes were obtained from the Mirai dataset and HELAD was executed on each trace. In Fig. 12a, we show the results for first 200,000 packets of each traces. In Fig. 12b, we also compare the expected anomaly scores (produced by HELAD in the original trace) and the predicted anomaly scores for each tampered trace. The results show that the anomaly scores produced by HELAD for the original and tampered traces overlap with each other and therefore, the scores do not have a significant dependence on the volume of the attack traffic encountered. Since the dots for tampered traces are close to the diagonal line in Fig. 12b, tampering with the Mirai attack traces had limited outcome on the predicted anomaly scores. This experiment demonstrates that the Mirai use case from HELAD is not vulnerable to variable packet rate samples to a significant extent.

E. Comparative Analysis

In this sub-section, we use *xAI evaluation metrics* to quantify the effectiveness of the explanations generated for the DL-based NIDSs under consideration by TRUSTEE and kernel SHAP. We use those metrics to compare the explanations across NIDSs. Currently, the existing implementations of objective *xAI* evaluation metrics as explained in Section III-B support kernel SHAP only and none of the implementations support TRUSTEE. TRUSTEE’s implementation comes with its own metric called *fidelity* which quantifies how accurate the TRUSTEE DT is with respect to the original black-box ML model. We also use the TRUSTEE-SHAP agreement scores



(a) Predicted anomaly score vs packet count



(b) Predicted vs expected anomaly score (produced by HELAD in the original trace)

Fig. 12: HELAD anomaly scores for the first 200k packets from original and tampered traces.

proposed in Section IV-B to compare the level of agreement between TRUSTEE DT and kernel SHAP explanations generated for the DL-based NIDSs considered.

TRUSTEE Fidelity: Using the Mirai dataset, if we compare the fidelity values obtained for the NIDSs considered, without any pruning, the highest fidelity values are obtained for Kitsune (0.786) out of the four NIDSs. With top-k pruning ($k = 10$), the highest fidelity values are obtained for Kitsune (0.721) out of the four NIDSs. Since ENIDrift, HorusEye and HELAD NIDSs yield negative and zero fidelity values, TRUSTEE DT explanations do not serve much purpose. Since top-k pruning is required to reduce the complexity of DT explanations and make them practical for cyber security personnel, *TRUSTEE is most useful for explaining the decisions of Kitsune NIDS*.

Using the CICIDS-2017 dataset, if we compare the fidelity values obtained for the NIDSs considered (refer Appendix Section A), without any pruning, the highest fidelity values are obtained for ENIDrift (0.929) out of the four NIDSs. With top-k pruning ($k = 10$), the highest fidelity values are obtained for Kitsune (0.919) out of the four NIDSs. Since HorusEye and HELAD NIDSs yield negative and zero fidelity values, TRUSTEE DT explanations do not serve much purpose. With top-k pruning, *TRUSTEE is most useful for explaining the decisions of Kitsune NIDS followed by ENIDrift NIDS*. Across the datasets, with top-k pruning, *Kitsune NIDS yields the*

highest fidelity values. The comparison of fidelity values obtained during TRUSTEE analysis of the DL-based NIDSs considered in this paper is shown in Table V.

NIDS Name	Fidelity (Without pruning)		Fidelity (with top-k pruning, k=10)	
	Mirai dataset	CICIDS-2017 dataset	Mirai dataset	CICIDS-2017 dataset
Kitsune	0.786	0.843	0.721	0.919
HorusEye	-1.365	-0.956	-1.038e-06	-0.018
ENIDrift	0.715	0.929	-1.536e-09	0.53
HELAD	0.0	0.0	0.0	0.0

TABLE V: Comparison of TRUSTEE fidelity values with and without pruning for DL-based NIDSs considered

SHAP evaluation metrics: We experimented with multiple implementations of objective xAI evaluation metrics (e.g., completeness, faithfulness, stability, monotonicity) to compare the kernel SHAP explanations across the four NIDSs evaluated in our experiments. Some of those implementations are OpenXAI¹, XAI-bench² and Quantus³. However, after extensive experimentation with those implementations, we found out that none of them support custom ML models such as those used for NIDSs. They support out-of-the-box ML models such as linear regression, MLP and ANN only.

Level of TRUSTEE-SHAP Agreement: We set the value of $m = 3$ for the m -point average TRUSTEE-SHAP agreement score. Each of the data subsets used for calculation of TRUSTEE-SHAP agreement scores were required to have a minimum number of 300 samples. The results are shown in Table VI. HorusEye, with a score of 0.381, exhibits the highest level of TRUSTEE-SHAP agreement, followed by Kitsune, with a score of 0.167 while ENIDrift has a score of 0.0. We also find that the TRUSTEE-SHAP agreement scores obtained for an NIDS for the different data subsets vary significantly. For example, for Kitsune, the scores obtained for three different data subsets were 0.4, 0.6 and 0.1. This supports our earlier assumption that the level of agreement between TRUSTEE DT explanation and SHAP explanation for a blackbox NIDS model may depend on the specific data subset which is used to conduct the TRUSTEE-SHAP comparison.

NIDS	m -point avg. TRUSTEE-SHAP agreement score (m=3)
Kitsune	0.167
HorusEye	0.381
ENIDrift	0.0
HELAD	n/a

TABLE VI: Comparison of m -point average TRUSTEE-SHAP agreement scores for DL-based SOTA NIDSs trained with Kitsune Mirai dataset

VI. DISCUSSION AND FUTURE WORK

From the experimental results obtained in the previous section, we have seen that *some DL-based NIDS models (Kitsune, ENIDrift) can be better interpreted in terms of decision*

trees than other models (HorusEye, HELAD). This might be attributed to the complexity of the NIDS model architecture and the properties of the model components. For example, HorusEye NIDS fidelity values are in the negative. Though HorusEye architecture includes only a single autoencoder in the second stage (which processes control plane traffic) compared to an ensemble of AEs in Kitsune or ENIDrift, that single AE is modified from a conventional AE to keep it lightweight, reduce the computational complexity, reduce the false-positive rate and improve throughput. It uses an asymmetric AE with separable convolution, dilation convolution and model quantization. As it is, AEs are limited in their interpretability as a result of their non-linear nature. Due to the complex architecture of the modified AE deployed in HorusEye, TRUSTEE might not be able to build a DT which can imitate the decisions of the black-box modified AE within an acceptable error rate. Therefore, to build DL-based NIDSs with better “explainability”, we recommend using less complex DL architectures and conventional components. However, there will be a trade-off between “explainability” and model performance (e.g., false-positive rate) and NIDS designers need to achieve a balance between the two.

We have also seen from the results that *TRUSTEE and SHAP explanations are in conflict for 2 out of 3 DL-based NIDSs considered in our work*. Their explanations are in agreement for HorusEye NIDS but in conflict for Kitsune and ENIDrift NIDSs. This is probably due to the fact that SHAP value for each feature is calculated for a subset of data samples and reflects the importance of that feature in the decision made by the black-box model for a majority of the data samples in that subset. On the other hand, TRUSTEE acts on the complete input dataset and identifies the top features contributing the most to forming the decision boundary separating all benign and malicious data samples which are part of the input dataset. Another reason could be the different optimization criteria used by TRUSTEE and SHAP while building explanations. TRUSTEE applies a teacher-student dynamic derived from imitation learning that uses the black-box ML/DL model as an oracle in conjunction with a carefully curated dataset to guide the training of a surrogate “white-box” model in the form of a DT that imitates the black-box’s decisions. On the other hand, SHAP uses the Shapley kernel method to approximate the black-box model-interpretable model fidelity function which recovers Shapley values. The specific data subset used to conduct the TRUSTEE-SHAP comparison could also play a role in the conflict. To reduce the conflict between TRUSTEE and SHAP explanations at the subset-level, we need to further investigate its underlying cause in the future.

Finally, it can be inferred from the results that *some DL-based NIDSs (Kitsune) are more vulnerable to variable packet rate samples than others (HorusEye, HELAD) while for the rest (ENIDrift), such vulnerability remains inconclusive*. One of the possible underlying reasons is that sometimes NIDSs are trained with training data containing higher than real-world attack traffic volume. To reduce vulnerability to variable packet rate samples, we recommend that NIDS designers use training data which reflects the attack traffic volume in real-world deployments. Additionally, the NIDS architecture

¹<https://github.com/AI4LIFE-GROUP/OpenXAI>

²<https://github.com/abacusai/xai-bench>

³<https://github.com/understandable-machine-intelligence-lab/Quantus>

may also have a role to play in its vulnerability to variable packet rate samples. An AE trained on benign traffic may be vulnerable to attack traffic with variable packet rates as the threshold used for output loss function (RMSE) is determined based on “in-distribution” attack traffic present in the training data. Since, Kitsune consists of an ensemble of AEs, the vulnerability effect is amplified. HorusEye consists of a single modified AE and therefore, its vulnerability to variable packet rate samples is not as pronounced as Kitsune. ENIDrift uses a different method of feature extraction (vector embedding) and updates the weights assigned to AEs in the ensemble based on change in attack traffic distribution which might keep it from producing a discernable pattern of dependence on attack traffic volume compared to Kitsune. We have observed earlier that HELAD NIDS anomaly scores are not vulnerable to variable packet rate samples to a significant extent. This may be attributed to HELAD’s architecture which combines an AE with an LSTM network. Since the final anomaly score is a weighted exponential aggregation of AE’s actual RMSE score and LSTM’s predicted RMSE scores for future samples (using historical samples). Even if the AE is vulnerable to variable packet rate samples, the LSTM’s predicted RMSE scores might be much larger compared to the AE’s RMSE score (the exponential operation makes the value even larger), thus affecting the final anomaly score to a greater extent and reducing HELAD’s vulnerability to variable packet rate samples.

VII. CONCLUSION

We have analyzed four state-of-the-art DL-based NIDS models (Kitsune, HorusEye, ENIDrift, HELAD) using explainable AI techniques such as TRUSTEE and SHAP. Using both global explanations and local explanations for the black-box models’ decisions, we have presented the most prominent features used by each NIDS model considered. We have compared the explanations generated across xAI methods for a given NIDS model (using our devised data subset-level explanation approach) as well as the explanations generated across the NIDS models for a given xAI method (using fidelity and other standard evaluation metrics). Finally, we evaluate the vulnerability of each NIDS model to inductive bias (variable packet rate samples). The results show that: (1) some DL-based NIDS models can be better interpreted in terms of decision trees than other models, (2) TRUSTEE and SHAP explanations are in conflict for most of the NIDS models considered in this work and (3) some NIDS models are more vulnerable to variable packet rate samples than other models.

REFERENCES

- [1] V. Paxson, “Bro: a system for detecting network intruders in real-time,” in *Proceedings of the 7th Conference on USENIX Security Symposium - Volume 7*, ser. SSYM’98. USA: USENIX Association, 1998, p. 3.
- [2] M. Roesch, “Snort - Lightweight Intrusion Detection for Networks,” in *Proceedings of the 13th USENIX Conference on System Administration*, ser. LISA ’99. USA: USENIX Association, 1999, p. 229–238.
- [3] D. Chou and M. Jiang, “A Survey on Data-driven Network Intrusion Detection,” *ACM Comput. Surv.*, vol. 54, no. 9, oct 2021. [Online]. Available: <https://doi.org/10.1145/3472753>
- [4] R. Sommer and V. Paxson, “Outside the Closed World: On Using Machine Learning for Network Intrusion Detection,” in *2010 IEEE Symposium on Security and Privacy*, May 2010, pp. 305–316.
- [5] Y. Mirsky, T. Doitshman, Y. Elovici, and A. Shabtai, “Kitsune: An Ensemble of Autoencoders for Online Network Intrusion Detection,” in *25th Annual Network and Distributed System Security Symposium, NDSS 2018, San Diego, California, USA, February 18-21, 2018*. The Internet Society, 2018. [Online]. Available: http://wp.internetsociety.org/ndss/wp-content/uploads/sites/25/2018/02/ndss2018_03A-3_Mirsky_paper.pdf
- [6] D. Arp, E. Quiring, F. Pendlebury, A. Warnecke, F. Pierazzi, C. Wressnegger, L. Cavallaro, and K. Rieck, “Dos and Don’ts of Machine Learning in Computer Security,” in *31st USENIX Security Symposium (USENIX Security 22)*. Boston, MA: USENIX Association, Aug. 2022, pp. 3971–3988. [Online]. Available: <https://www.usenix.org/conference/usenixsecurity22/presentation/arp>
- [7] A. S. Jacobs, R. Beltiukov, W. Willinger, R. A. Ferreira, A. Gupta, and L. Z. Granville, “AI/ML for Network Security: The Emperor has no Clothes,” in *Proceedings of the 2022 ACM SIGSAC Conference on Computer and Communications Security*, ser. CCS ’22. New York, NY, USA: Association for Computing Machinery, 2022, p. 1537–1551. [Online]. Available: <https://doi.org/10.1145/3548606.3560609>
- [8] S. M. Lundberg and S.-I. Lee, “A unified approach to interpreting model predictions,” in *Proceedings of the 31st International Conference on Neural Information Processing Systems*, ser. NIPS’17. Red Hook, NY, USA: Curran Associates Inc., 2017, p. 4768–4777.
- [9] F. Ceschin, M. Botacin, A. Bifet, B. Pfahringer, L. S. Oliveira, H. M. Gomes, and A. Grégio, “Machine Learning (In) Security: A Stream of Problems,” *Digital Threats*, vol. 5, no. 1, mar 2024. [Online]. Available: <https://doi.org/10.1145/3617897>
- [10] G. Apruzzese, P. Laskov, and J. Schneider, “SoK: Pragmatic Assessment of Machine Learning for Network Intrusion Detection,” in *2023 IEEE 8th European Symposium on Security and Privacy (EuroS&P)*. Los Alamitos, CA, USA: IEEE Computer Society, jul 2023, pp. 592–614. [Online]. Available: <https://doi.ieeeecomputersociety.org/10.1109/EuroSP57164.2023.00042>
- [11] R. Kalakoti, H. Bahsi, and S. Nömm, “Improving IoT Security With Explainable AI: Quantitative Evaluation of Explainability for IoT Botnet Detection,” *IEEE Internet of Things Journal*, vol. 11, no. 10, pp. 18 237–18 254, 2024.
- [12] S. Patil, V. Varadarajan, S. M. Mazhar, A. Sahibzada, N. Ahmed, O. Sinha, S. Kumar, K. Shaw, and K. Kotecha, “Explainable Artificial Intelligence for Intrusion Detection System,” *Electronics*, vol. 11, no. 19, 2022. [Online]. Available: <https://www.mdpi.com/2079-9292/11/19/3079>
- [13] O. Arreche, T. R. Guntur, J. W. Roberts, and M. Abdallah, “E-XAI: Evaluating Black-Box Explainable AI Frameworks for Network Intrusion Detection,” *IEEE Access*, vol. 12, pp. 23 954–23 988, 2024.
- [14] P. Barnard, N. Marchetti, and L. A. DaSilva, “Robust Network Intrusion Detection Through Explainable Artificial Intelligence (XAI),” *IEEE Networking Letters*, vol. 4, no. 3, pp. 167–171, 2022.
- [15] M. T. Ribeiro, S. Singh, and C. Guestrin, “‘Why Should I Trust You?’: Explaining the Predictions of Any Classifier,” ser. KDD ’16. New York, NY, USA: Association for Computing Machinery, 2016. [Online]. Available: <https://doi.org/10.1145/2939672.2939778>
- [16] B. Ingre and A. Yadav, “Performance analysis of NSL-KDD dataset using ANN,” in *2015 International Conference on Signal Processing and Communication Engineering Systems*, 2015, pp. 92–96.
- [17] I. Sharafaldin, A. H. Lashkari, and A. A. Ghorbani, “Toward Generating a New Intrusion Detection Dataset and Intrusion Traffic Characterization,” in *Proceedings of the 4th International Conference on Information Systems Security and Privacy - Volume 1: ICISPP, INSTICC*. SciTePress, 2018, pp. 108–116.
- [18] A. Warnecke, D. Arp, C. Wressnegger, and K. Rieck, “Evaluating Explanation Methods for Deep Learning in Security,” in *2020 IEEE European Symposium on Security and Privacy (EuroS&P)*. Los Alamitos, CA, USA: IEEE Computer Society, sep 2020, pp. 158–174. [Online]. Available: <https://doi.ieeeecomputersociety.org/10.1109/EuroSP48549.2020.00018>
- [19] M. Wang, K. Zheng, Y. Yang, and X. Wang, “An Explainable Machine Learning Framework for Intrusion Detection Systems,” *IEEE Access*, vol. 8, pp. 73 127–73 141, 2020.
- [20] M. M. Shtayat, M. K. Hasan, R. Sulaiman, S. Islam, and A. U. R. Khan, “An Explainable Ensemble Deep Learning Approach for Intrusion Detection in Industrial Internet of Things,” *IEEE Access*, vol. 11, pp. 115 047–115 061, 2023.

- [21] T. Zebin, S. Rezvy, and Y. Luo, “An Explainable AI-Based Intrusion Detection System for DNS Over HTTPS (DoH) Attacks,” *IEEE Transactions on Information Forensics and Security*, vol. 17, pp. 2339–2349, 2022.
- [22] C. Minh, K. Vermeulen, C. Lefebvre, P. Owezarski, and W. Ritchie, “An Explainable-by-Design Ensemble Learning System to Detect Unknown Network Attacks,” in *2023 19th International Conference on Network and Service Management (CNSM)*, 2023, pp. 1–9.
- [23] E. Alhajjar, P. Maxwell, and N. Bastian, “Adversarial machine learning in Network Intrusion Detection Systems,” *Expert Systems with Applications*, vol. 186, p. 115782, 2021. [Online]. Available: <https://www.sciencedirect.com/science/article/pii/S0957417421011507>
- [24] M. Chalé, B. Cox, J. Wier, and N. D. Bastian, “Constrained optimization based adversarial example generation for transfer attacks in network intrusion detection systems,” *Optimization Letters*, vol. 18, pp. 2169–2188, 2021.
- [25] L. S. Shapley, *17. A Value for n-Person Games*. Princeton: Princeton University Press, 1953, pp. 307–318. [Online]. Available: <https://doi.org/10.1515/9781400881970-018>
- [26] W. Guo, D. Mu, J. Xu, P. Su, G. Wang, and X. Xing, “LEMNA: Explaining Deep Learning based Security Applications,” in *Proceedings of the 2018 ACM SIGSAC Conference on Computer and Communications Security*, ser. CCS ’18. New York, NY, USA: Association for Computing Machinery, 2018, p. 364–379. [Online]. Available: <https://doi.org/10.1145/3243734.3243792>
- [27] L. Coroama and A. Groza, “Evaluation Metrics in Explainable Artificial Intelligence (XAI),” in *Advanced Research in Technologies, Information, Innovation and Sustainability*, T. Guarda, F. Portela, and M. F. Augusto, Eds. Cham: Springer Nature Switzerland, 2022, pp. 401–413.
- [28] Y. Dong, Q. Li, K. Wu, R. Li, D. Zhao, G. Tyson, J. Peng, Y. Jiang, S. Xia, and M. Xu, “HorusEye: A Realtime IoT Malicious Traffic Detection Framework using Programmable Switches,” in *32nd USENIX Security Symposium (USENIX Security 23)*. Anaheim, CA: USENIX Association, Aug. 2023, pp. 571–588. [Online]. Available: <https://www.usenix.org/conference/usenixsecurity23/presentation/dong-yutao>
- [29] X. Wang, “ENIDrift: A Fast and Adaptive Ensemble System for Network Intrusion Detection under Real-world Drift,” in *Proceedings of the 38th Annual Computer Security Applications Conference*, ser. ACSAC ’22. New York, NY, USA: Association for Computing Machinery, 2022, p. 785–798. [Online]. Available: <https://doi.org/10.1145/3564625.3567992>
- [30] Y. Zhong, W. Chen, Z. Wang, Y. Chen, K. Wang, Y. Li, X. Yin, X. Shi, J. Yang, and K. Li, “HELAD: A novel network anomaly detection model based on heterogeneous ensemble learning,” *Computer Networks*, vol. 169, p. 107049, 2020. [Online]. Available: <https://www.sciencedirect.com/science/article/pii/S1389128619304086>

APPENDIX A MORE EXPERIMENTAL RESULTS

In this section, we present explanations of the four state-of-the-art DL-based NIDSs (Kitsune, HorusEye, ENIDrift, HELAD) generated using xAI methods such as TRUSTEE and kernel SHAP where the NIDSs were trained/tested with the CICIDS-2017 dataset.

A. Case Study- Kitsune × CICIDS-2017

TRUSTEE Analysis: The results of TRUSTEE analysis for Kitsune are shown in Table VII. Using TRUSTEE with 30% of the original CICIDS-2017 dataset samples and no pruning results in the DT explanation which achieves 0.843 fidelity compared to Kitsune. Using TRUSTEE with 30% of the dataset samples and top-k Pruning method (setting $k = 3$) results in a DT explanation that is shown in Fig. 13 and achieves 0.919 fidelity compared to Kitsune.

The top three prominent features that Kitsune uses to determine an anomaly are: $HpHp_0.1_pcc_0_1$, $HH_0.1_pcc_0_1$ and $HH_jit_0.01_std$. Thus, Kitsune relies mainly on the sizes

of packets and the jitter experienced by packets exchanged per time frame to determine if an attack is underway.

Sample size	Top-k pruning used?	DT size, depth, leaves	Fidelity
30%	No	78819, 80, 39410	0.843
30%	Yes (k=3)	29, 14, 15	0.919

TABLE VII: TRUSTEE analysis results for Kitsune CICIDS-2017 model

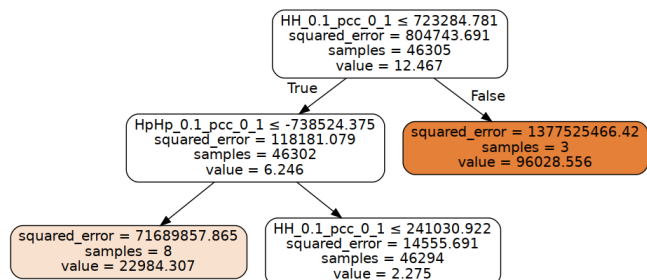


Fig. 13: Decision tree for Kitsune CICIDS-2017 model with Top-k pruning (k=3). Only the top 3 layers are shown.

SHAP Analysis: Using kernel SHAP analysis, Fig. 14 shows a summary of how the top features in CICIDS-2017 dataset impact the Kitsune NIDS model’s output through a beeswarm plot for randomly selected 1000 data samples corresponding to the benign root node-leaf node path in the TRUSTEE DT (Fig. 13). Features such as $HpHp_0.01_weight_0$, $HH_jit_0.01_weight$ and $HH_0.01_weight_0$ have the most impact on the prediction value, in that order.

TRUSTEE vs SHAP Analysis: Using the systematic approach for comparing TRUSTEE and SHAP explanations as explained in sub-section IV-B, since the set of features used in the benign root node-leaf node path in the TRUSTEE DT is not a subset of the set of top contributing features computed by kernel SHAP summary analysis ($HpHp_0.1_pcc_0_1$ is the only common feature between the two sets), *TRUSTEE AND SHAP explanations do not agree with each other at the subset level for Kitsune NIDS.*

Detection of Inductive Bias: The CICIDS-2017 dataset does not provide a separate dataset for botnet traffic trace which could be used for comparison with the Mirai trace in terms of the attack traffic volume. However, using a similar approach for tampering as in the case of Mirai trace, we evaluated the following threshold ranges (in packets per second) for ARP requests originating from infected hosts : (1) 10-50, (2) 30-70 and (3) 50-90. The original trace as well as the tampered traces are shown in Fig. 15. It can be observed that: (1) there is no significant difference between the benign and attack traffic volumes for the original trace and (2) tampering had negligible effect on the difference between benign and attack traffic in terms of number of packets per second. Thus, unlike the Mirai trace, there is no significant difference between the benign and attack traffic volumes which can be learnt by the NIDS model and leave it vulnerable to a change in attack traffic distribution. Thus, we do not investigate the presence of inductive bias (vulnerability to variable packet rate samples) any further for NIDS models trained with the CICIDS-2017 dataset.

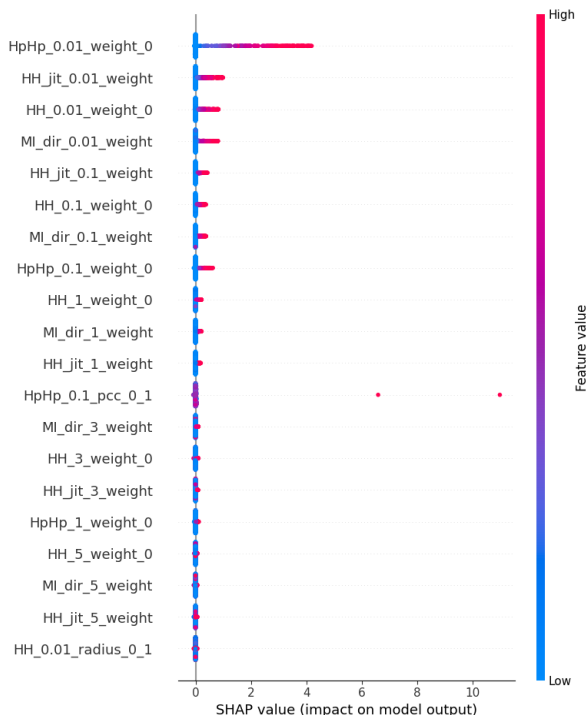


Fig. 14: SHAP beeswarm plot for Kitsune CICIDS-2017 model

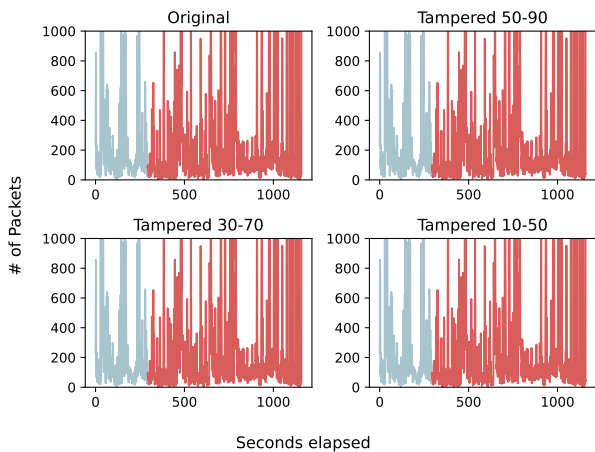


Fig. 15: Number of packets per second for original CICIDS-2017 trace and tampered traces. Blue portions of the plot correspond to benign traffic while red portions correspond to malicious traffic inclusive of benign and attack traffic.

B. Case Study- HorusEye \times CICIDS-2017

TRUSTEE Analysis: The results of TRUSTEE analysis for HorusEye are shown in Table VIII. Using TRUSTEE with 30% of the CICIDS-2017 dataset samples with no pruning results in a DT explanation which achieves negative fidelity (~ -0.956) compared to original HorusEye model. Using TRUSTEE with 30% of the dataset samples and top-k Pruning method (setting $k = 10$) results in a DT explanation which achieves negative fidelity (~ -0.018) compared to original HorusEye model but higher fidelity compared to no pruning. Negative fidelity values mean that the DT explanation fits HorusEye predictions worse than the mean of the predictions.

Nevertheless, the decision tree for HorusEye Mirai model

with top-k pruning ($k=10$) is shown in Fig. 16. The top three prominent features that HorusEye’s DT uses to determine an anomaly are: $HH_5_pcc_0_1$, $HpNet_1_covariance_0_1$ and $HH_jit_0.01_std$. Thus, HorusEye’s DT relies mainly on the sizes of packets and the jitter experienced by packets exchanged between a pair of IP addresses per time frame to determine if an attack is underway.

Sample size	Top-k pruning used?	DT size, depth, leaves	Fidelity
30%	No	20265, 94, 10133	-0.956
30%	Yes ($k=10$)	241, 52, 121	-0.018

TABLE VIII: TRUSTEE analysis results for HorusEye CICIDS-2017 model

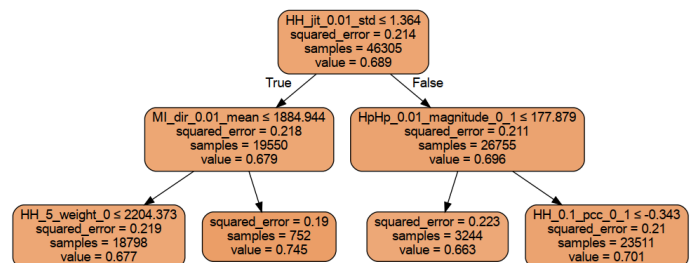


Fig. 16: Decision tree for HorusEye CICIDS-2017 model with Top-k pruning ($k=10$). Only the top 3 layers are shown.

SHAP Analysis: Using kernel SHAP analysis, Fig. 17 shows a summary of how the top features in CICIDS-2017 dataset impact the HorusEye NIDS model’s output using a beeswarm plot for randomly selected 1000 data samples corresponding to the benign root node-leaf node path in the TRUSTEE DT (Fig. 16). Features such as $HH_jit_0.1_std$, $MI_dir_0.01_std$ and $HpNet_0.1_weight_0$ have the most impact on the prediction value, in that order.

TRUSTEE vs SHAP Analysis: Using the systematic approach for comparing TRUSTEE and SHAP explanations as explained in sub-section IV-B, the set of features used in the benign root node-leaf node path in the TRUSTEE DT is not a subset of the set of top contributing features computed by kernel SHAP summary analysis. Therefore, *TRUSTEE AND SHAP explanations do not agree with each other at the subset level for HorusEye NIDS.*

C. Case Study- ENIDrift \times CICIDS-2017

In this analysis, we used the CICIDS-2017-Wed (corresponding to the CICIDS data collected on July 5, 2017 (Wednesday)) dataset for training/testing ENIDrift NIDS.

TRUSTEE Analysis: The results of TRUSTEE analysis for ENIDrift are shown in Table IX. Using TRUSTEE with 30% of the CICIDS-2017 dataset samples and no pruning results in the DT explanation which achieves 0.929 fidelity compared to ENIDrift. Using TRUSTEE with 30% of the dataset samples and top-k Pruning method (setting $k = 10$) results in a DT explanation (shown in Fig. 18) which achieves 0.53 fidelity compared to ENIDrift. This is expected since pruning the branches of a DT reduces its fidelity. The most prominent features ENIDrift uses to determine anomaly are: $f38$, $f81$, $f158$.

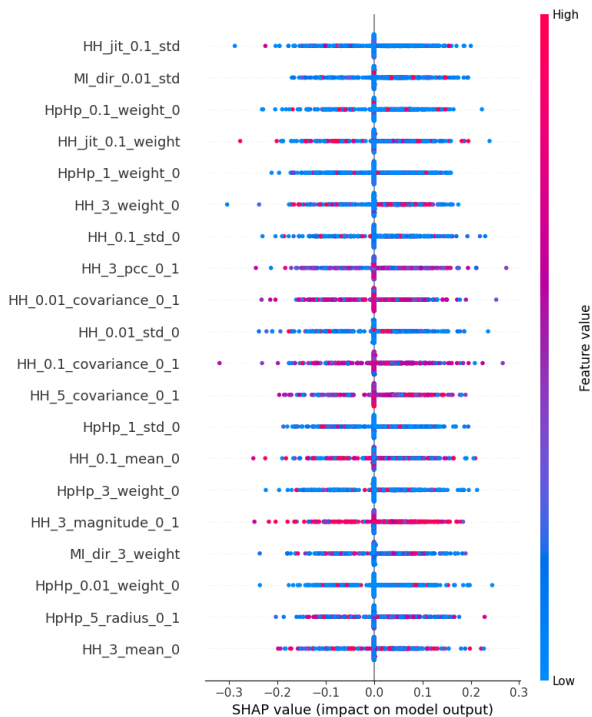


Fig. 17: SHAP beeswarm plot for HorusEye CICIDS-2017 model

Sample size	Top-k pruning used?	DT size, depth, leaves	Fidelity
30%	No	253, 24, 127	0.929
30%	Yes (k=10)	25, 7, 13	0.53

TABLE IX: TRUSTEE analysis results for ENIDrift CICIDS-2017 model

SHAP Analysis: Fig. 19 shows a summary of how the top features in CICIDS-2017 dataset impact the ENIDrift NIDS model's output using a beeswarm plot for randomly selected 300 data samples. Features (embedding vector components) such as f_{31} , f_{84} , f_{155} have the most impact on the prediction value, in that order.

TRUSTEE vs SHAP Analysis: Using the systematic approach for comparing TRUSTEE and SHAP explanations as explained in sub-section IV-B, the set of features used in the benign root node-leaf node path in the TRUSTEE DT is not a subset of the set of top contributing features computed by kernel SHAP summary analysis (there are no common features between the two sets). Therefore, *TRUSTEE AND SHAP explanations do not agree with each other at the subset level for ENIDrift NIDS.*

D. Case Study- HELAD \times CICIDS-2017

In this analysis, we used a subset of the original CICIDS-2017 dataset consisting of 301,000 packets for this analysis as per the open source implementation⁴ released by the authors. The first 200,000 packets were used for training and the rest of the packets were used for testing. Among the packets used for testing, the first 50,000 were benign while the rest were attack-related. The complete CICIDS-2017 dataset was not used since it increased the LSTM training time substantially.

⁴<https://github.com/cdogemaru/CPiP>

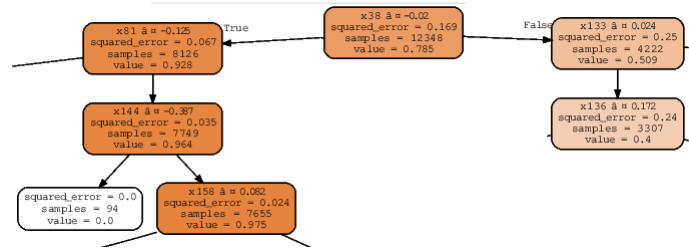


Fig. 18: Decision tree for ENIDrift CICIDS-2017 model with Top-k pruning (k=10). Only the top 4 layers are shown.

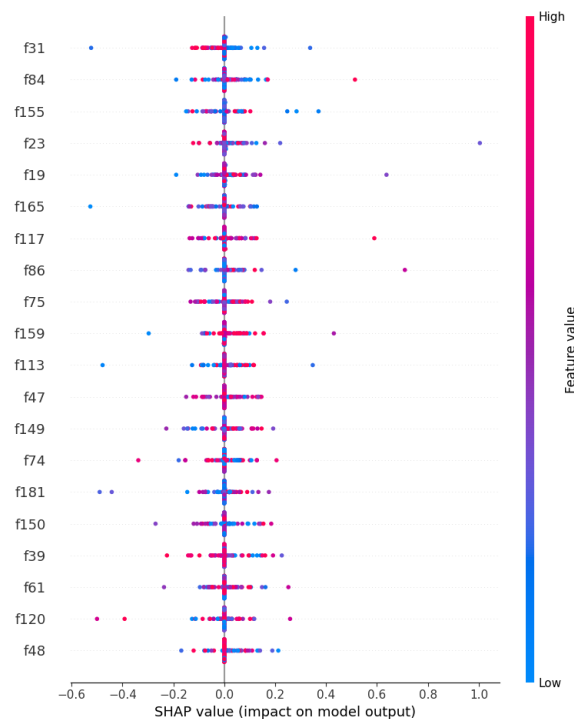


Fig. 19: SHAP beeswarm plot for ENIDrift CICIDS-2017 model

TRUSTEE Analysis: The results of TRUSTEE analysis for HELAD are shown in Table X. Using TRUSTEE with 30% of the reduced CICIDS-2017 dataset samples and no pruning results in the DT explanation which achieves 0.0 fidelity compared to HELAD. Using TRUSTEE with 30% of the dataset samples and top-k Pruning method (setting $k = 10$) results in a DT explanation (shown in Fig. 20) which achieves 0.0 fidelity compared to HELAD.

The top three prominent features HELAD's DT uses to determine an anomaly are:

- 1) $HH_jit_0.01_mean$ - Packet jitter aggregated by traffic sent between a set of source and destination IP addresses with time window 0.01 (1 minute).
- 2) $HH_0.1_radius_0_1$ - L2-norm of variances of two packet size streams aggregated by traffic sent between a set of source and destination IP addresses with time window 0.1 (10 seconds).
- 3) $MI_dir_1.0_std$ - Standard deviation of packet sizes aggregated by source MAC and IP addresses, with time window 1.0 (1.5 seconds).

Thus, *HELAD's DT relies mainly on the jitter experienced and*

the sizes of packets exchanged between a pair of IP addresses per time frame to determine if an attack is underway.

Sample size	Top-k pruning used?	DT size, depth, leaves	Fidelity
30%	No	19607, 94, 9804	0.0
30%	Yes (k=10)	475, 77, 238	0.0

TABLE X: TRUSTEE analysis results for HELAD NIDS

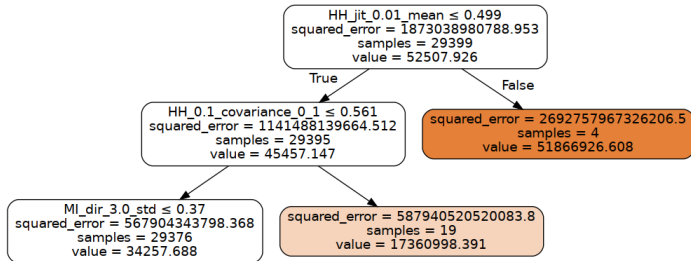


Fig. 20: Decision tree for HELAD CICIDS-2017 model with Top-k pruning (k=10). Only the top 3 layers are shown.

SHAP Analysis: Running a kernel SHAP analysis of HELAD NIDS with the reduced CICIDS-2017 dataset resulted in issues. First, we ran the analysis with 200,000 packets but it threw a *numpy* memory error since it was unable to allocate a huge amount of memory (313 GiB) for storing a (2248×20000000) array with 64-bit float values. Next, we ran the analysis with 20,000 packets but the LSTM was taking too long to train. Hence, we decided to not proceed with the kernel SHAP analysis.